



HAL
open science

Empirical Run-Time Bias Correction for Antarctic Regional Climate Projections With a Stretched-Grid AGCM

Gerhard Krinner, Julien Beaumet, Vincent Favier, Michel Deque, Claire Brutel-Vuilmet

► **To cite this version:**

Gerhard Krinner, Julien Beaumet, Vincent Favier, Michel Deque, Claire Brutel-Vuilmet. Empirical Run-Time Bias Correction for Antarctic Regional Climate Projections With a Stretched-Grid AGCM. Journal of Advances in Modeling Earth Systems, 2019, 11 (1), pp.64-82. 10.1029/2018MS001438 . hal-02105273

HAL Id: hal-02105273

<https://hal.science/hal-02105273>

Submitted on 1 Sep 2021

HAL is a multi-disciplinary open access archive for the deposit and dissemination of scientific research documents, whether they are published or not. The documents may come from teaching and research institutions in France or abroad, or from public or private research centers.

L'archive ouverte pluridisciplinaire **HAL**, est destinée au dépôt et à la diffusion de documents scientifiques de niveau recherche, publiés ou non, émanant des établissements d'enseignement et de recherche français ou étrangers, des laboratoires publics ou privés.



Distributed under a Creative Commons Attribution - NonCommercial - NoDerivatives 4.0 International License



RESEARCH ARTICLE

10.1029/2018MS001438

Empirical Run-Time Bias Correction for Antarctic Regional Climate Projections With a Stretched-Grid AGCM

Gerhard Krinner¹ , Julien Beaumet¹, Vincent Favier¹, Michel Déqué², and Claire Brutel-Vuilmet¹¹CNRS, Université Grenoble Alpes, Institut des Géosciences de l'Environnement (IGE), Grenoble, France, ²CNRM, Université de Toulouse, Météo-France, CNRS, Toulouse, France**Key Points:**

- Empirical run-time bias correction is used in a variable-resolution AGCM for projections of the Antarctic climate
- Present-day mean climate and its interannual and high-frequency variability are improved in the bias-corrected AGCM runs
- This method is a promising complementary approach for a more consistent end-to-end climate change modeling chain including impact modeling

Correspondence to:G. Krinner,
gerhard.krinner@cnrs.fr**Citation:**Krinner, G., Beaumet, J., Favier, V., Déqué, M., & Brutel-Vuilmet, C. (2019). Empirical run-time bias correction for Antarctic regional climate projections with a stretched-grid AGCM. *Journal of Advances in Modeling Earth Systems*, 11, 64–82. <https://doi.org/10.1029/2018MS001438>

Received 11 JUL 2018

Accepted 22 DEC 2018

Accepted article online 28 DEC 2018

Published online 11 JAN 2019

Abstract This work presents snapshot simulations of the late 20th and late 21st century Antarctic climate under the RCP8.5 scenario carried out with an empirically bias-corrected global atmospheric general circulation model (AGCM), forced with bias-corrected sea-surface temperatures and sea ice and run with about 100-km resolution over Antarctica. The bias correction substantially improves the simulated mean late 20th century climate. The simulated atmospheric circulation of the bias-corrected model compares very favorably to the best available AMIP (Atmospheric Model Intercomparison Project)-type climate models. The simulated interannual circulation variability is improved by the bias correction. Depending on the metric, a slight improvement or degradation is found in the simulated variability on synoptic timescales. The simulated climate change over the 21st century is broadly similar in the corrected and uncorrected versions of the atmospheric model, and atmospheric circulation patterns are not geographically “pinned” by the applied bias correction. These results suggest that the method presented here can be used for bias-corrected climate projections. Finally, the authors discuss different possible choices in terms of the place of bias corrections and other intermediate steps in the modeling chain leading from global coupled climate simulations to impact assessment.

Plain Language Summary Climate models are necessary and irreplaceable tools for climate projections, but despite continuous improvement, they still have biases, and their spatial resolution is too low to provide actionable climate change information at relevant small spatial scales. We present a method combining bias corrections and high-resolution climate modeling that allows improving climate projections at regional scales.

1. Introduction

Global climate models are the fundamental tools used for projecting future climate change (Collins et al., 2013). However, given their limited spatial resolution, their output usually needs to be downscaled to regional and smaller scales (Hall, 2014) before it can be used for climate change impact studies. Because all global climate models exhibit biases (Flato et al., 2013; Gleckler et al., 2008), bias correction is usually applied at some point in the work flow that leads from the global climate model to impact assessment via a downscaling step (Maraun, 2016). In most cases, bias correction (also termed bias adjustment) is conflated with statistical downscaling of global or regional climate model output in order to provide input for an impact model (Maraun et al., 2017). Such bias-adjusted downscaled climate change projections are widely available and used in a wide range of impact studies and assessment reports (Maraun et al., 2017).

At what point of the treatment the bias correction is applied tends to depend on the type of downscaling that is chosen. Dynamical downscaling (e.g., Giorgi & Gutowski, 2015; Gutowski et al., 2016) consists of driving a regional, high-resolution limited-area climate model at its lateral boundaries with high-frequency (a few hours), three-dimensional atmospheric state variables and fluxes from a global climate model. Usually, these driving data are not bias corrected, because the instantaneous three-dimensional wind, temperature, and humidity-driving fields need to be mutually consistent, which places difficult constraints on bias correction. As a consequence, the computationally cost-intensive limited area models are usually driven with uncorrected, biased atmospheric forcing from climate models. This fact is referred to as the “garbage in-garbage out” problem of regional-scale climate projections (e.g., Hall,

©2018. The Authors.

This is an open access article under the terms of the Creative Commons Attribution-NonCommercial-NoDerivs License, which permits use and distribution in any medium, provided the original work is properly cited, the use is non-commercial and no modifications or adaptations are made.

2014; Rummukainen, 2010); here the word “garbage” must of course not be interpreted as an expression of a lack of respect for the work of climate model developers over several decades. Bias correction is then usually applied to the RCM output.

Statistical downscaling methods (Hewitson et al., 2014) often involve a bias correction of the climate model data they use as input; this is often possible because the driving data are not three-dimensional, at somewhat lower temporal resolution, and usually comprise less variables than in the case of dynamical downscaling.

Bias correction of (regional or global) climate model output in the context of climate change studies is necessarily based on the hypothesis that the climate model biases are either stationary or at least related to the simulated climate in a reproducible way (e.g., Kerkhoff et al., 2014). On small scales, which are particularly relevant for statistical bias correction methods, bias stationarity of variables such as near-surface temperature and precipitation has been shown to be frequently insufficient for simple bias correction methods to be applied (Chen et al., 2015; Haerter et al., 2011; Teutschbein & Seibert, 2013). Therefore, empirical bias correction of climate model simulations at run time, based on the analysis of present-day climate model biases, has preferentially been applied in the context of seasonal climate prediction (Guldberg et al., 2005; Kharin & Scinocca, 2012) and not for projections of climate change. However, in spite of the absence of a rigorous justification of the underlying fundamental hypothesis of bias stationarity, a posteriori bias corrections of atmospheric AOGCM (atmosphere-ocean general circulation model) output have been carried out to produce lateral driving data for climate change studies with regional climate models (Bruyère et al., 2013; Done et al., 2015; Patricola & Cook, 2010; Xu & Yang, 2012).

An alternative approach to driving a regional climate model directly with bias-corrected AOGCM output consists of using an atmospheric general circulation model (AGCM) driven by bias-corrected ocean boundary conditions (OBC; sea-surface temperatures [SST] and sea-ice concentration [SIC]). This approach has been taken by Krinner et al. (2008, 2014), Ashfaq et al. (2011), and Hernández-Díaz et al. (2017). These studies show clear improvements of the simulated current climate because observed lower OBC are used instead of biased AOGCM OBC. Bias correction of OBC is, at least at first sight, more straightforward than that of lateral boundary conditions for a RCM, because OBC for AGCMs are only two-dimensional surface fields and evolve less rapidly in time than three-dimensional atmospheric driving variables, which are typically updated at a 6-hourly time step. Krinner et al. (2014) and Hernández-Díaz et al. (2017) argue in favor of a three-step downscaling approach that consists of using output of these atmospheric GCM simulations, driven by bias-corrected OBC, as driving data for further downscaling with regional, limited-area climate models. If a stretched-grid AGCM with regional high resolution is used, such as in Krinner et al. (2014), and the AGCM used skillfully simulates the surface climate of the region considered, the last step consisting of driving a regional climate model with the AGCM output might not be necessary at all.

In any case, all these approaches rely to some degree on the fundamental hypothesis of climate model bias stationarity. Krinner and Flanner (2018) recently showed that large-scale tropospheric climate model bias patterns do indeed tend to be highly stationary under strong climate change. This suggests that empirical bias correction of climate model simulations at run time (or a posteriori) is justifiable in the context of climate projections, because the underlying strong hypothesis of bias stationarity is supported.

Here we present and evaluate climate simulations for the end of the 20th century and projections for the end of the 21st century focused on the Antarctic region carried out with an empirically bias-corrected atmospheric general circulation model, using an atmospheric correction in addition to bias-corrected OBC. It is thus an extension of the three-step downscaling approach proposed by Krinner et al. (2014) and Hernández-Díaz et al. (2017), which only use bias-corrected OBC: Our study here also includes an empirical atmospheric bias correction applied at run time in the AGCM. We will argue that this run-time atmospheric bias correction can be used as an alternative or, preferably, complement to a posteriori bias corrections of AOGCM output.

This work is intended as a proof of concept for future studies of Antarctic climate change with a bias-corrected atmospheric general circulation model. However, the methods described here can be readily applied to any other region of the planet, or globally. The main purpose of this paper is to provide an assessment of the impact of atmospheric bias corrections on the present-day and future large-scale Antarctic climate as simulated by an atmospheric general circulation model with relatively high resolution over the Antarctic region. In the following section, we first present the method of bias correction applied here and the simulation setup. Section 3 will analyze the results of the simulations for the end of the 20th and the

end of the 21st century. The analysis concerns, on one hand, large-scale circulation features of the Southern circumpolar climate. On the other hand, we assess the simulated Antarctic climate and its change as such. We will analyze in some detail the effect of the bias correction on the simulated Antarctic precipitation change, because precipitation is the principal driver of interannual variability of the surface mass balance of the Antarctic ice sheet (e.g., Shepherd et al., 2018). Furthermore, it is projected to be the most important driver of future Antarctic surface mass balance changes (Agosta et al., 2013; Cornford et al., 2015). As an important component of global sea level change, Antarctic precipitation is therefore of particular interest. Methodological issues, possible applications, and perspectives will be discussed in section 4. In particular, we assess the potential for using this kind of simulations to drive regional climate models.

2. Methods

2.1. Bias Correction Method

We apply an empirical bias correction method that has been described by Guldberg et al. (2005) and more recently used by Kharin and Scinocca (2012). The approach consists of two steps. The first step is a nudged simulation (Jeuken et al., 1996) in which the local model solution for selected prognostic variable X is modified at each model time step by applying a Newtonian relaxation to a time-varying reference state X_R (we use the notation by Kharin and Scinocca, 2012, in the following):

$$\frac{\partial X}{\partial t} = F(X) - \frac{1}{\tau} (X - X_R), \quad (1)$$

where X is the nudged solution, $F(X)$ is the original (not nudged) prognostic evolution of variable X , and τ is a time constant of the order of typically about 6 hr. The time-varying reference state is usually taken from atmospheric (re)analyses.

The climatological seasonal cycle of the applied correction terms is then calculated:

$$G = -\frac{1}{\tau} \overline{(X_N - X_R)}^{AC}. \quad (2)$$

As in Kharin and Scinocca (2012), the operator $\overline{(\cdot)}^{AC}$ stands for the annual cycle of X . These climatological but seasonally and spatially varying correction terms G correspond to the mean initial model drift away from atmospheric conditions close to observed states. They are therefore not necessarily proportional to the climatological mean biases one aims to reduce with this approach, but Transpose-AMIP experiments (Ma et al., 2014) have shown that there is often a good correspondence between mean short-term forecast errors and climate errors in climate models. We apply a 30-day running-mean smoothing, preserving the mean daily cycle, to calculate the seasonal cycle of the correction terms. In a second simulation, these terms are then added to the prognostic equations:

$$\frac{\partial X}{\partial t} = F(X) + G. \quad (3)$$

This yields an empirically bias-corrected solution X . This type of bias correction, consisting of introducing a prescribed correction term in the right-hand side of a prognostic model equation, is also often referred to as “flux correction” (Collins et al., 2006; Dommenges & Rezný, 2018; Irvine et al., 2013), especially in coupled models where the correction was often applied at the ocean-atmosphere interface (Manabe & Stouffer, 1988; Sausen et al., 1988), thereby directly changing the fluxes between the model components.

The time constant τ of the Newtonian relaxation is 6 hr above the atmospheric boundary layer. Below $\sigma = 0.85$ (corresponding to about 850 hPa in regions with low surface elevation), the nudging strength rapidly decreases ($\tau \rightarrow \infty$), leaving the surface variables to evolve freely. We use the ERA-Interim reanalysis (Dee et al., 2011) for nudging the zonal and meridional wind speeds and the atmospheric temperature for the period 1979–2000. ERA-Interim data are frequently used to drive regional climate models, notably in the CORDEX exercise (Gutowski et al., 2016), and can therefore be considered as a standard for similar applications. The bias correction terms are then deduced from the nudging tendencies for the period 1980–2000.

Table 1
Simulations Analyzed in This Work

Simulation	Type, atmospheric correction	Period, scenario, and ocean boundary conditions
R20	Free, uncorrected	1979–2000; observed OBC
N20	Nudged to ERA-INT	1979–2000; observed OBC
C20	Free, bias-corrected	1979–2000; observed OBC
R21	Free, uncorrected	2079–2100; RCP8.5; debiased IPSL-CM5 OBC
C21	Free, bias-corrected	2079–2100; RCP8.5; debiased IPSL-CM5 OBC

Note. OBC = ocean boundary conditions.

2.2. Model Setup

We use LMDZ5 (Hourdin et al., 2013), a global atmospheric general circulation model (AGCM), that is the atmospheric component of the IPSL coupled model (Dufresne et al., 2013). The LMDZ5 grid point AGM is here set up with 96 (longitude) \times 95 (latitude) grid points, 39 vertical levels, and a meridionally stretched grid refined over the Antarctic, yielding a meridional grid point spacing of slightly above 100 km in the Antarctic region, compared to up to 290 km in the Northern Hemisphere. Grid spacing is regular (3.75°) in the zonal direction, with a zonal filtering of small spatial scales near the pole due to convergence of the meridians, preventing effective zonal resolution from exceeding the maximum meridional resolution. This setup allows to carry out simulations of the Antarctic climate at relatively high spatial resolution at a very moderate cost and to simulate two-way atmospheric interactions with regions further north, because the model remains a global one.

OBC (SST, SIC, and sea-ice thickness) have to be prescribed because we use an atmospheric model. We used observed SST and sea ice concentrations for the “present” (1979–2000) period from Rayner et al. (2003). For the projection runs for the 21st century, the required OBC are obtained by applying the bias correction method described by Beaumet et al. (2017), in which the SST and SIC change projected by a coupled climate model (here IPSL-CM5) is applied to historical observed OBC. This means that we only use the SST and SIC change that is projected by a coupled climate model (here IPSL-CM), not its present-day simulated SST and SIC. Therefore, our simulations are not affected by SST and SIC biases of the coupled model or by errors in simulated trends over the historical period. Here we use the period 1979–2000 from the CMIP5 historical run, the period 2079–2100 from CMIP5 RCP8.5 run, and the 1979–2000 observed (Rayner et al., 2003) boundary conditions. Sea-ice thickness is diagnosed from instantaneous and annual maximum SIC following Beaumet et al. (2017). Atmospheric composition (greenhouse gases, aerosols, and ozone) is prescribed following the CMIP5 protocol.

2.3. Simulations

We carried out 5 LMDZ5 simulations for this work. The free, uncorrected reference run for the late 20th century (1979–2000) is noted R20. The nudged simulation of the late 20th century (1979–2000) climate will be referred to as N20 in the remainder of the paper. The bias-corrected simulation for the same period, using the nudging tendencies from N20, is called C20. All three 20th-century simulations (R20, N20, and C20; see Table 1) use prescribed observed SST and sea ice concentrations (Rayner et al., 2003).

Two simulations of the late 21st century (2079–2100) are carried out for the RCP8.5 scenario: a free, uncorrected simulation (R21) that uses only bias-corrected OBC, but no empirical atmospheric bias correction, and a fully bias-corrected simulation (C21) that uses empirical atmospheric bias correction and corrected OBC. The bias-corrected late-21st century simulation C21 uses the same empirical atmospheric correction terms as C20.

The first year of each simulation is discarded as spin-up, leaving the 21 years from 1980 to 2000 and 2080 to 2100, respectively, for the analysis of R20, N20, C20, R21, and C21.

2.4. Analysis Methods

We use Kohonen’s self-organizing maps (SOMs; Kohonen, 1990; Kohonen & Honkela, 2007) to analyze the simulated dominant circulation patterns, in particular their changes between different model configurations and the impact of these changes on the simulated precipitation, as done in Krinner et al. (2014). SOMs are

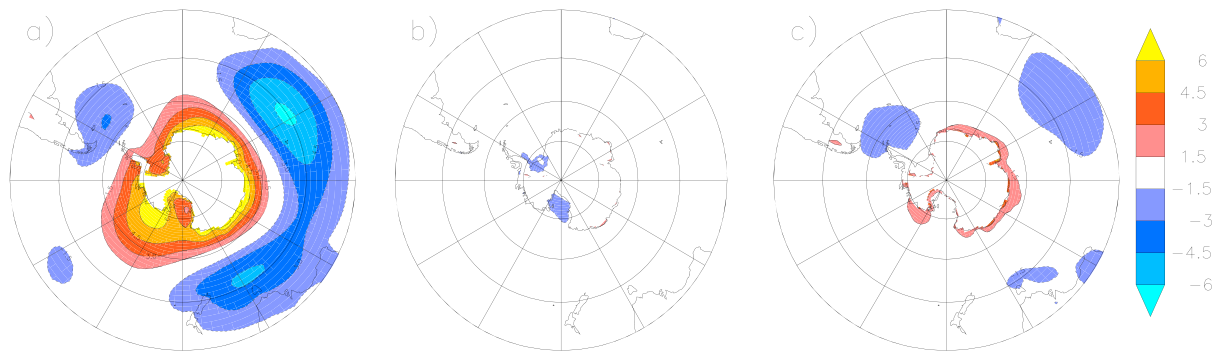


Figure 1. 1980–2000 annual mean sea-level pressure error with respect to ERA-INT (hPa). (a) R20, (b) N20, and (c) C20. Grid points with surface altitude above 1,000 m are masked.

based on an unsupervised machine-learning algorithm that, when applied to a series of daily sea level pressure maps, identifies a predefined number (here 20, ordered on a hexagonal 5×4 grid) of typical circulation patterns in this reference database. Depending on the application, these reference data are the output of a control simulation or of reanalyses. Each simulated daily sea level pressure pattern (from the same or another simulation) is then attributed to one of the identified typical circulation patterns, using the same distance metric that is also applied during the learning step.

Because the model is set up with a relatively high horizontal resolution over the Antarctic and the Southern Ocean and with low resolution further north, the analysis in the following concentrates on these regions. However, the nudging and the bias correction are applied globally, so the simulated atmospheric circulation is corrected also in the Northern Hemisphere.

The nudging time constant applied here globally above the planetary boundary layer ($\tau = 6$ hr) implies that the nudged simulation N20 closely follows the driving reanalysis on daily timescales and above, with almost identical variability patterns and magnitudes. Therefore, for some variables such as sea level pressure, N20 is in the following occasionally taken as an equivalent to an observational reference for convenience.

3. Results

3.1. Present Climate 1980–2000

3.1.1. Mean Climate

The annual mean sea level pressure bias in the uncorrected reference simulation R20 (Figure 1a) attains -6 hPa over the Southern Ocean. An opposite bias of the same magnitude appears closer to the Antarctic continent, particularly in the Amundsen Sea. Although atmospheric pressure is not assimilated in our nudging procedure—only wind and temperature are nudged—the pressure bias almost vanishes completely in N20 (Figure 1b). The bias-corrected simulation C20 exhibits very weak annual mean sea level pressure errors. Although the biases are much weaker in C20 than in R20, the geographical pattern of the remaining small errors (Figure 1c) resembles that of the errors of the uncorrected simulation R20, the error maxima being located in the same areas.

It is interesting to compare the simulated sea level pressure fields in the extratropical Southern Hemisphere with CMIP5 and coupled AMIP simulations. Agosta et al. (2015) assessed the Southern Hemisphere extratropical climate as simulated by a number of CMIP5 coupled models. Comparison of their Figure 1 with Figure 1 of this work shows, with little surprise, that the bias-corrected LMDZ5 model run exhibits weaker biases than all of the CMIP5 coupled models. This response is due in part to the use of observed OBC in our simulations, as opposed to (necessarily) imperfect simulated OBC in the coupled models, and in part to the empirical atmospheric bias correction applied here.

To isolate the effect of the empirical atmospheric bias correction, it is useful to compare our LMDZ5 simulations to the CMIP5 AMIP runs, which also use observed OBC. The simulated mean absolute annual mean sea level pressure error in the Southern Hemisphere extratropics (south of 30°S) of the bias-corrected LMDZ5 simulation C20 compares very favorably to the AMIP ensemble (Figure 2): Only

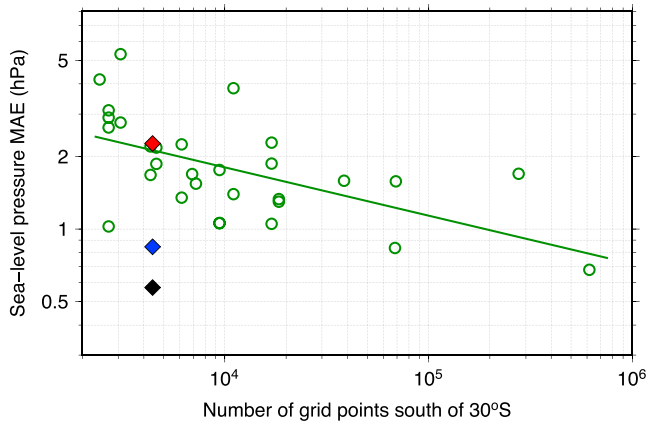


Figure 2. Areal-average mean absolute error (MAE, in hPa) of annual mean 1980–2000 sea-level pressure in AMIP-type AGCM simulations, with respect to ERA-Int. The areal average is calculated for all grid point south of 30°S with a surface elevation below 1,000 m. Green circles: CMIP5 AMIP simulations; black diamond: N20; blue diamond: C20; red diamond: R20. The green line represents a power regression on the AMIP data, with exponent $\beta = -0.20$.

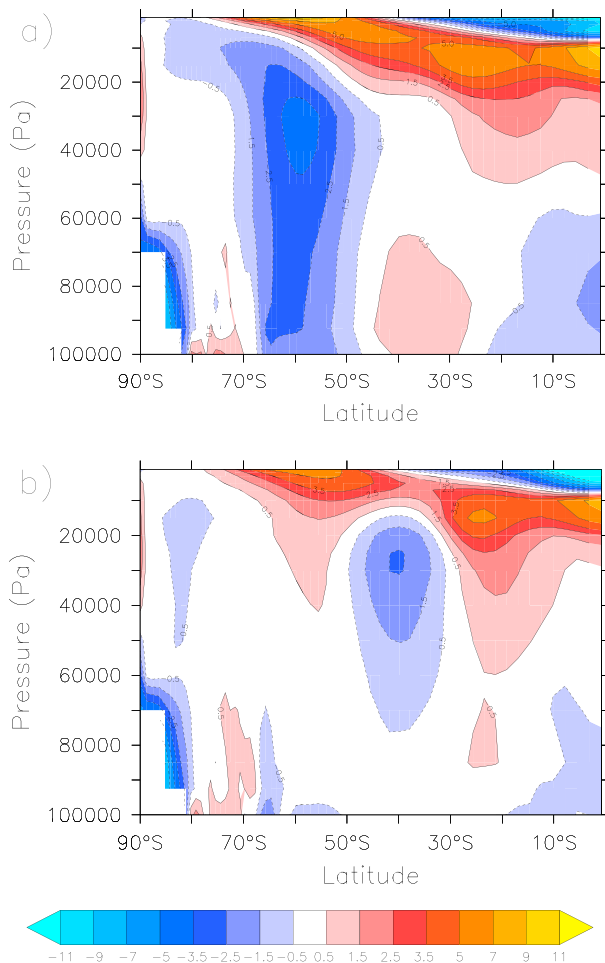


Figure 3. 1980–2000 annual mean zonal mean zonal wind error with respect to ERA-INT (m/s). (a) R20 and (b) C20.

the MRI-AGCM3-2S AGCM (Yukimoto et al., 2012), run at an exceptional horizontal resolution of 0.1875° , has a lower mean absolute error of 0.67 hPa south of 30°S , compared to 0.82 hPa for C20. Most models have mean absolute errors substantially above 1 hPa. There seems to be a tendency for lower biases at higher resolution, but a regression suggests that one typically has to increase the horizontal resolution by more than a factor of 5 to obtain a 50% bias reduction, and scatter is substantial. In spite of its rather low horizontal resolution, the bias magnitude of C20 is similar to that of the highest-resolution (about 25 km) AMIP run.

Similarly, the annual and zonal mean zonal wind errors (Figure 3) are substantially reduced in simulation C20 compared to R20 (we do not show output of simulation N20 for nudged fields, which are bias free by construction). In particular, the tropospheric bias reduction over the Southern Ocean is substantial, leading to an almost vanishing bias in that area. In the Northern Hemisphere, some biases continue to subsist (but these are weaker than in R20). This is probably linked to the very low model resolution in the Northern Hemisphere, which is not of particular interest here.

The reduction of the midtropospheric temperature errors (Figure 4 for January and Figure 5 for July) is again substantial. As seen for the pressure bias patterns, the temperature bias patterns in R20 and C20 are similar to some degree, with maxima and minima located in roughly the same areas.

In the annual mean, the uncorrected LMDZ model has a warm bias over the Antarctic continent, which is consistent with the warm summer and winter biases in the midtroposphere shown before. This also holds true for the near-surface climate. In the annual average over the continent, the bias-corrected simulation C20 is therefore 1.1°C cooler than R20 (-31.7°C instead of -30.6°C). The annual mean, continental mean precipitation rate is about 7% lower in C20 than in R20 (179 mm w.e./year instead of 193 mm w.e./year). The sensitivity S of the simulated continental mean accumulation A (defined as precipitation minus sublimation) to the surface air temperature difference ΔT between R20 and C20, calculated as $S = \Delta A / (\bar{A} \Delta T)$, where \bar{A} is the average accumulation between R20 and C20, is $8.7\%/^\circ\text{C}$. This is somewhat higher than typical values for the accumulation sensitivity to temperature reported in the context of climate change, which are mostly between $5\%/^\circ\text{C}$ and $7\%/^\circ\text{C}$ (Favier et al., 2017; Frieler et al., 2015; Krinner et al., 2008; e.g., Meehl et al., 2007), and which are, at first order, interpreted to be essentially linked to the temperature dependency of the atmosphere's moisture holding capacity. It appears therefore that the drying of the Antarctic atmosphere in the C20 simulation, compared to R20, is not only caused by the cooling induced by the bias correction method but that it is also substantially influenced by concomitant corrections to the atmospheric circulation. This is analyzed further in the section on short-term variability.

Atmospheric winds and temperature are, by construction, directly impacted by the bias correction procedure, which aims at reducing the mean error of these fields. As we have shown above, the mean errors of other atmospheric fields (e.g., surface pressure) are also positively affected. However, it is not obvious that emergent properties such as the

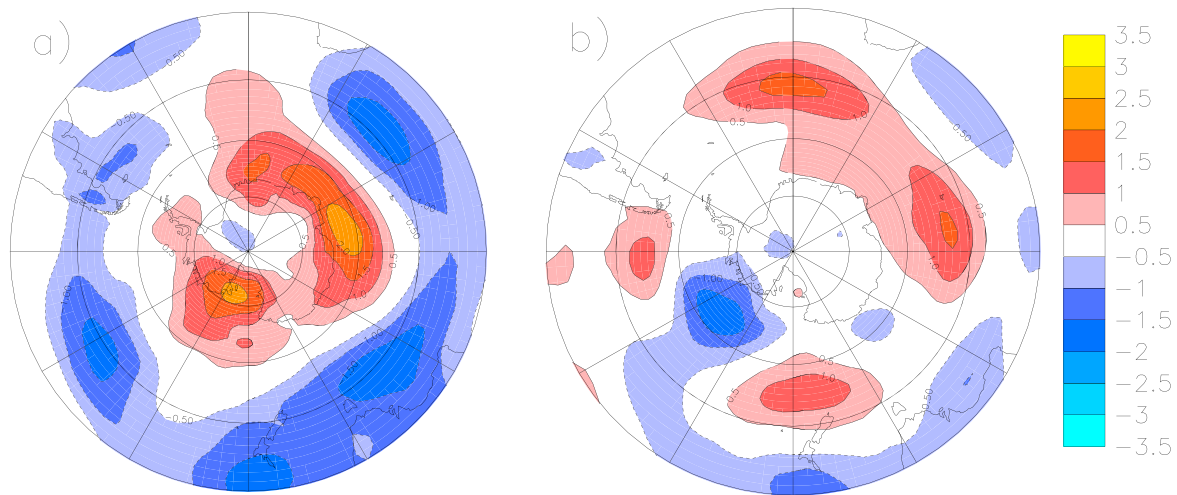


Figure 4. 1980–2000 January air temperature error at 500 hPa with respect to ERA-INT (°C). (a) R20 and *(b) C20.

interannual variability of the simulated atmospheric fields will be positively affected by the bias correction procedure. In the following, we will therefore analyze interannual and short-term variability in our simulations.

3.1.2. Interannual Variability

Interannual variability of the simulated atmospheric circulation is analyzed here in terms of empirical orthogonal functions (EOF). The dominant pattern, that is, the first EOF, corresponds to the Southern Annular Mode both in January (Figure 6) and in July (Figure 7). In July, the second and third EOFs (the latter not shown here) correspond to the two Pacific-South America patterns (PSA1 and PSA2; Mo & Higgins, 1998). With respect to N20, which is nudged to the reanalyses, the fraction of variance explained by the first EOF pattern (Table 2) in January is overestimated both in R20 (+19%) and C20 (+14%), but less so in C20. In July, C20 correctly estimates the fraction of variance associated to EOF1, while R20 substantially underestimates it (43% instead of 61%).

The geographic pattern of the second EOF in January (Figure 6) is incorrectly represented in the uncorrected simulation R20, while it is essentially correct in C20. In July, both R20 and C20 represent fairly correctly the geographic pattern of the second EOF. However, linked to its underestimating the variance associated to EOF1, the uncorrected simulation R20 overestimates the associated variance of EOF2.

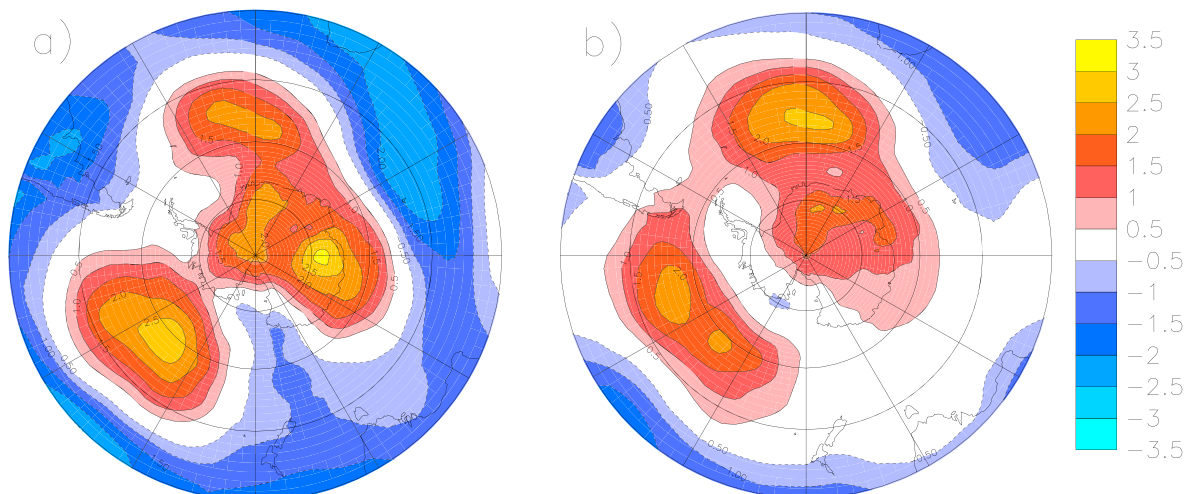


Figure 5. 1980–2000 July air temperature error at 500 hPa with respect to ERA-INT (°C). (a) R20 and (b) C20.

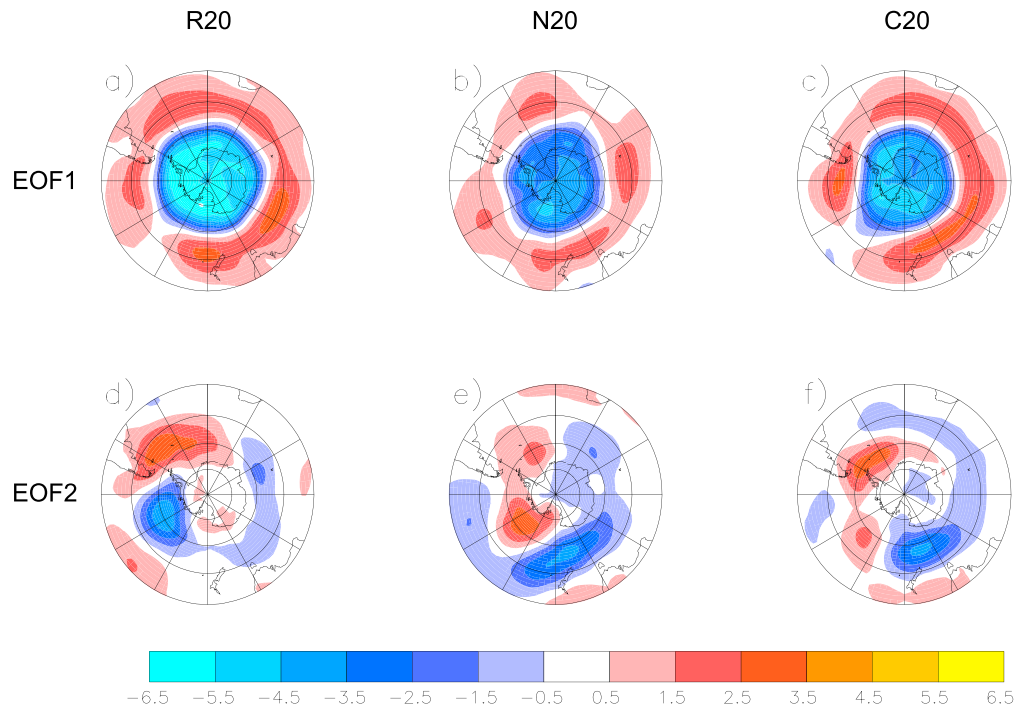


Figure 6. Empirical orthogonal function (EOF) of interannual variability of January sea-level pressure for the period 1980–2000. Top row (a–c): EOF1; bottom row (d–f): EOF2. From left to right: (a) and (d): R20; (b) and (e): N20; and (c) and (f): C20. N20, nudged to ERA-Int, is taken as the “observational” reference.

As a whole, interannual sea level pressure variability is somewhat better represented in the bias-corrected simulation C20 than in the uncorrected simulation R20.

3.1.3. Synoptic Variability

On shorter (synoptic) timescales, observed sea level pressure variability exhibits maxima centered at around 0°W and 90°W over the Southern Ocean (Figure 8b). LMDZ underestimates variability at these timescales, and more so in C20 (Figure 8c) than in R20 (Figure 8a). In particular, C20 underestimates the synoptic variability in the Eastern Pacific sector of the Southern Ocean. However, the global pattern of synoptic variability is correct both in R20 and C20, with stronger variability in the Atlantic and Pacific sectors than in the Indian Ocean sector.

This warrants a closer look at the ability of LMDZ, in its different configurations, to represent the Southern Hemisphere atmospheric circulation variability at short timescales: how well does LMDZ, in its different configurations, represent the typical Southern Hemisphere weather patterns and their respective frequencies? The 20 typical synoptic situations identified by applying Kohonen’s SOM method to daily ERA-20C sea level pressure data from January 1980 to December 2000 are displayed in Figure 9. The SOM algorithm automatically places similar synoptic situations close to each other on the predefined grid.

In ERA-20C, which can certainly be considered to be a trustworthy representation of the reality in term of large-scale circulation patterns in the lower troposphere for the period 1980–2000, these circulation patterns occur at frequencies between 3% and 8%, with no pattern or group of neighboring patterns dominating (gray bars in Figure 10). In the nudged simulation N20, the frequencies of the simulated situations are very similar, with a root mean square error (RMSE) of 1.0% (black bars in Figure 10). A slight deterioration is visible in C20, with a RMSE of 1.8%; however, there is no clear bias toward a coherent underestimation or overestimation of the frequencies of a specific group of synoptic situations. In R20, however, LMDZ suffers from a clear bias toward a systematic overestimate of the frequencies of the synoptic situations placed at the lower right edge of Figure 9 (situations 15, 19, and 20), characterized by a weak meridional pressure gradient. The overestimate is compensated for by an underestimate of other circulation patterns, particularly of those exhibiting a strong sea level pressure minimum in the

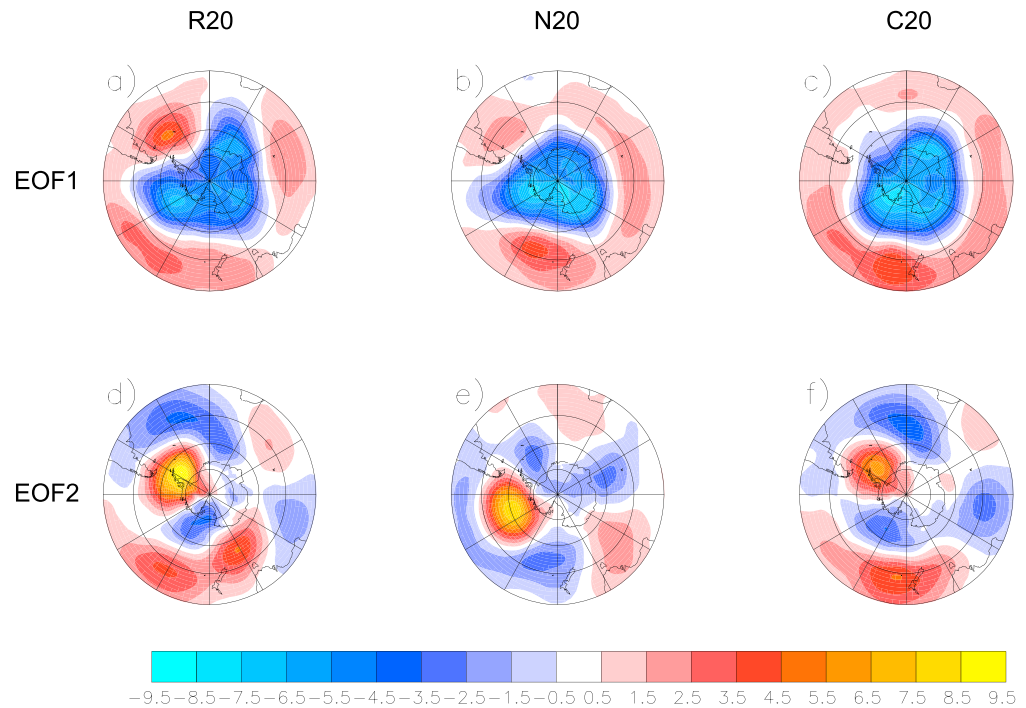


Figure 7. Empirical orthogonal function (EOF) of interannual variability of July sea-level pressure for the period 1980–2000. Top row (a–c): EOF1; bottom row (d–f): EOF2. From left to right: (a) and (d): R20; (b) and (e): N20; and (c) and (f): C20. N20, nudged to ERA-Int, is taken as the “observational” reference. For N20, the bottom row EOF vector (e) is actually the third EOF (variance explained for EOF2 and 3 in this case are 11% and 7%, respectively), chosen because it corresponds to EOF2 of R20 and C20.

Amundsen and Bellingshausen Seas (situations 6, 11, 12, and 16). This misfit is consistent with the mean sea level pressure bias of R20 shown before in Figure 1. The frequencies of these patterns are more realistic in the bias-corrected simulation C20. This is consistent with the correction of the mean sea level pressure bias shown in Figure 1. The bias correction thus improves both mean circulation and synoptic variability on the synoptic spatial scale.

The RMSE of the synoptic pattern occurrences in R20 is 2.9%, which is much higher than for C20 (1.8%). In fact, a fairly high number of synoptic situations in R20 are not well represented by the SOMs built from the ERA-20C sea level pressure data; these are attributed to maps on the fringes of the SOM grid (patterns 15, 19, and 20 in Figure 9, leading to high numbers of occurrences for these maps in R20) not because these fits are good, but simply because these are the least inappropriate fits. In these cases, the simulated sea level pressure distribution in R20 is typically even more uniform than in these extreme maps 15, 19, and 20.

Table 2
Fraction of Interannual Variance of Sea-Level Pressure Explained by EOFs 1 and 2 (in %)

	R20	N20	C20
EOF1, January	77	58	72
EOF2, January	5	10	6
EOF1, July	43	61	61
EOF2, July	21	7	10

Note. EOF = empirical orthogonal function. For July, EOF3 (7% variance explained) is listed for N20 instead of EOF2, which explains 11% of the variance (as in Figure 7). N20, nudged to ERA-Int, is taken as the “observational” reference.

LMDZ overestimates the average duration of these typical synoptic situations, that is, the average number of consecutive days during which the synoptic situation stays in a given configuration corresponding to one of the 20 identified patterns. While this average duration is 1.8 days in ERA-20C, it is 2.1 days in N20 and C20, and 2.2 days in R20. This is consistent with the underestimate of the Southern Hemisphere high-frequency circulation variability already shown in Figure 8. However, judging from this metric, C20 is slightly more realistic than R20.

These circulation changes caused by the bias correction impact the simulated Antarctic precipitation rates. Following Krinner et al. (2014), the simulated mean precipitation \bar{P} can be written as a sum, over all $N = 20$ circulation patterns, of the fraction of time a given

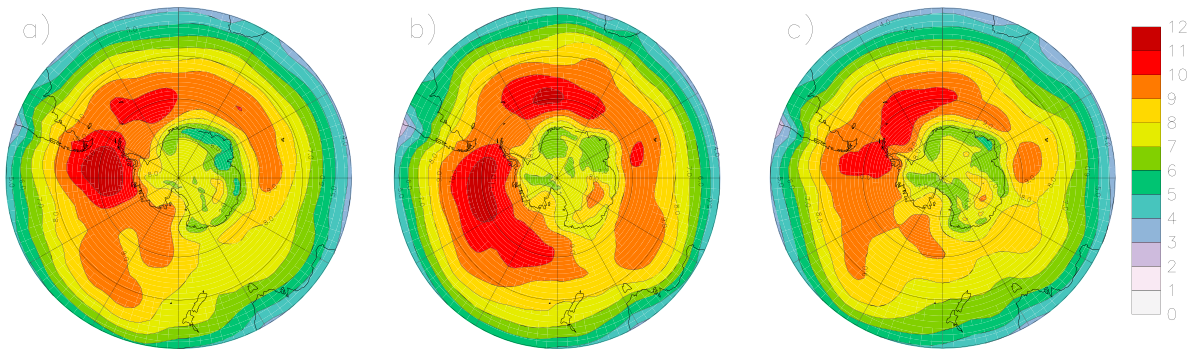


Figure 8. Standard deviation of high-pass (10-day) filtered daily sea-level pressure in July (hPa), 1980 to 2000. (a) R20, (b) N20, and (c) C20.

circulation pattern occurs (f_k) times the mean precipitation rate simulated during times at which this pattern occurs ($\overline{P_k}$):

$$\overline{P} = \sum_{k=1}^N (f_k \cdot \overline{P_k}). \quad (4)$$

The mean precipitation change between two simulations (here R20 and C20) can then be decomposed following, Driouech et al. (2010): Defining $\Delta \overline{P}_k = \overline{P_{C20,k}} - \overline{P_{R20,k}}$ and $\Delta f_k = f_{C20,k} - f_{R20,k}$ allows us to write

$$\begin{aligned} \Delta \overline{P} &= \overline{P_{C20}} - \overline{P_{R20}} = \sum_{k=1}^N (f_{C20,k} \cdot \overline{P_{C20,k}}) - \sum_{k=1}^N (f_{R20,k} \cdot \overline{P_{R20,k}}) \\ &= \sum_{k=1}^N ((f_{R20,k} + \Delta f_k) \cdot \overline{P_{C20,k}}) + \sum_{k=1}^N (f_{R20,k} \cdot (\overline{P_{C20,k}} - \Delta \overline{P}_k)) \\ &= \sum_{k=1}^N (f_{R20,k} \cdot \Delta \overline{P}_k) + \sum_{k=1}^N (\overline{P_{C20,k}} \cdot \Delta f_k). \end{aligned} \quad (5)$$

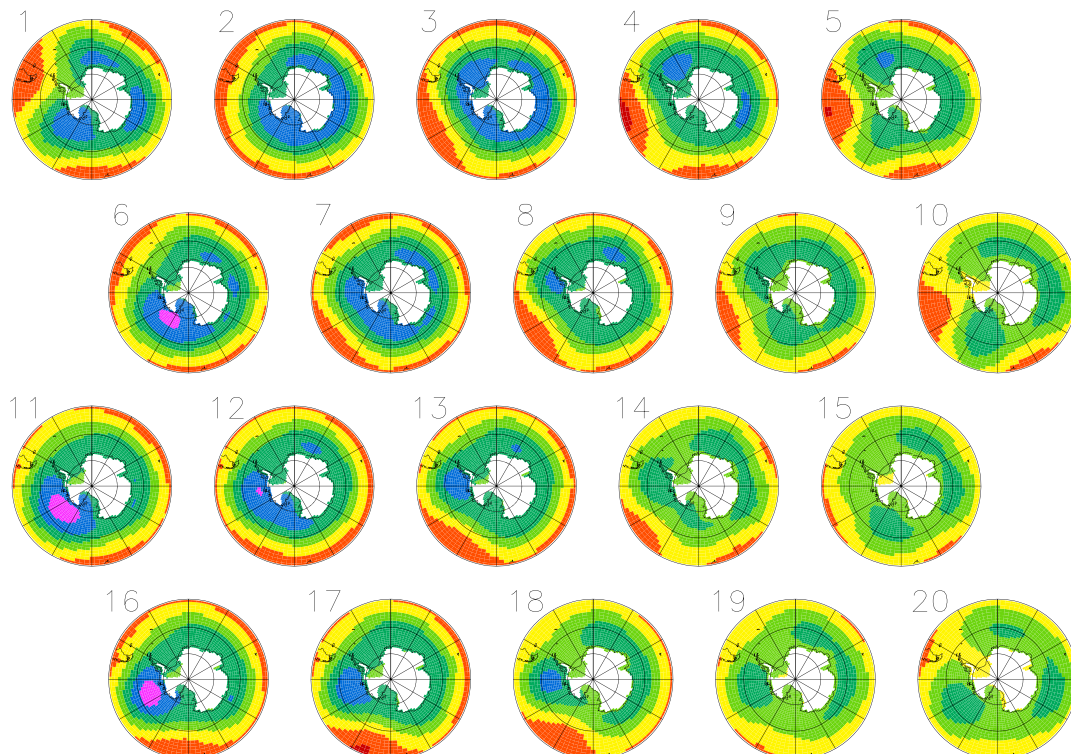


Figure 9. Self-organizing maps of 20 representative daily sea-level pressure situations for ERA-20C, 1980 to 2000.

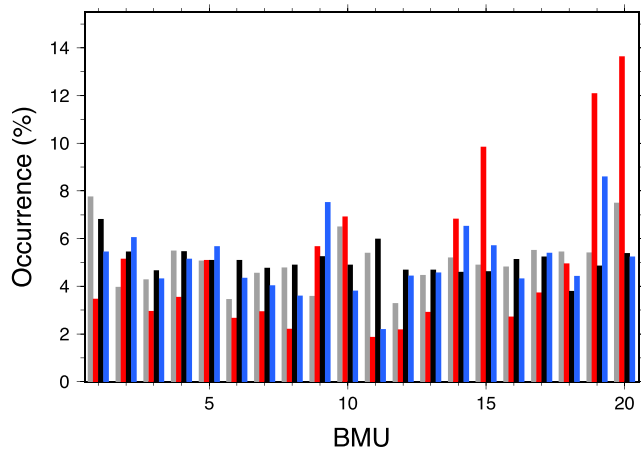


Figure 10. Frequencies of occurrence (%) of the 20 typical meteorological situations (“Best Matching Units,” BMU) shown in Figure 9 for ERA-20C (gray), N20 (black), C20 (blue), and R20 (red).

by a cyclonic system in the Amundsen Sea area, which are represented in the left-wing panels of Figure 9. Increased advection of oceanic air toward the Peninsula leads to a strong precipitation increase in C20. This is consistent with the increased strength of the Amundsen Sea Low shown in Figure 1 and with the increased frequency of synoptic situations characterized by low pressure in the Amundsen Sea shown in Figure 10. A similar important role for circulation corrections, evidenced by the local dominance of the S_{pdf} component (Figure 11c) in the total precipitation change signal (Figure 11a), is visible in coastal Enderby Land. However, over the largest part of the continent, and in particular inland, modified mean precipitation rates for given synoptic situation tend to be the dominant cause for precipitation changes, as can be deduced from the fact that the S_{fdp} signal (Figure 11b) is broadly rather similar to the total precipitation change (Figure 11a). This finding is consistent with the mean cooling in C20 compared to R20, which reduces the moisture holding capacity of the air.

3.2. Climate Projections: Late 21st Versus Late 20th Century

In this section, we will analyze the simulated climate change from the late 20th (1980–2000) to the late 21st century (2080–2100) under the RCP8.5 scenario, focusing on processes and variables potentially affecting the simulated surface mass balance of the Antarctic ice sheet.

The bias correction in C20 leads to a southward displacement and intensification of the Southern Ocean low pressure belt, as can be seen in Figure 12: In the simulation C20, which is very weakly biased (see also Figure 1), the trough is deepened by about 3 hPa and shifted by about 2° latitude to the South compared to R20. The same southward shift and intensification also occurs in the two 21st century simulations R21

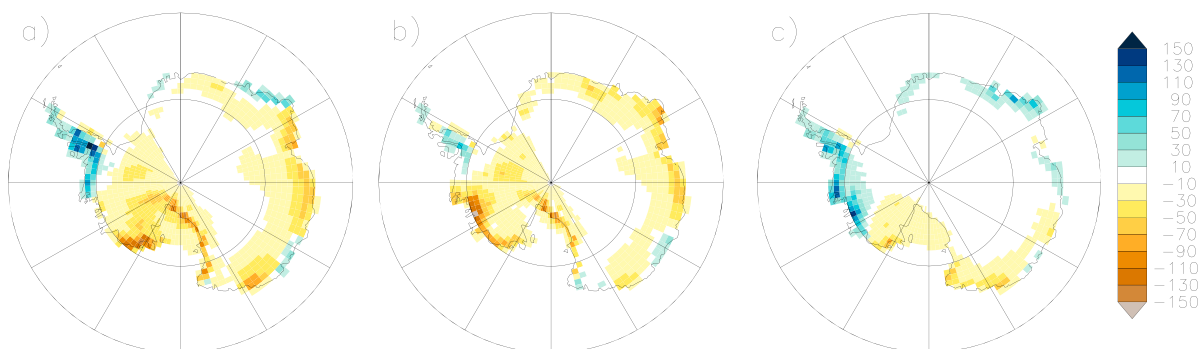


Figure 11. Annual mean precipitation change $\Delta\bar{P} = \overline{P_{C20}} - \overline{P_{R20}}$ over the Antarctic ice sheet induced by the bias correction (i.e., the difference C20 minus R20), and its components ($\text{kg}\cdot\text{m}^{-2}\cdot\text{year}^{-1}$). (a) Annual mean precipitation difference, (b) $S_{fdp} = \sum_{k=1}^N (f_{R20,k} \cdot \Delta\bar{P}_k)$, and (c) $S_{pdf} = \sum_{k=1}^N (\overline{P_{C20,k}} \cdot \Delta f_k)$.

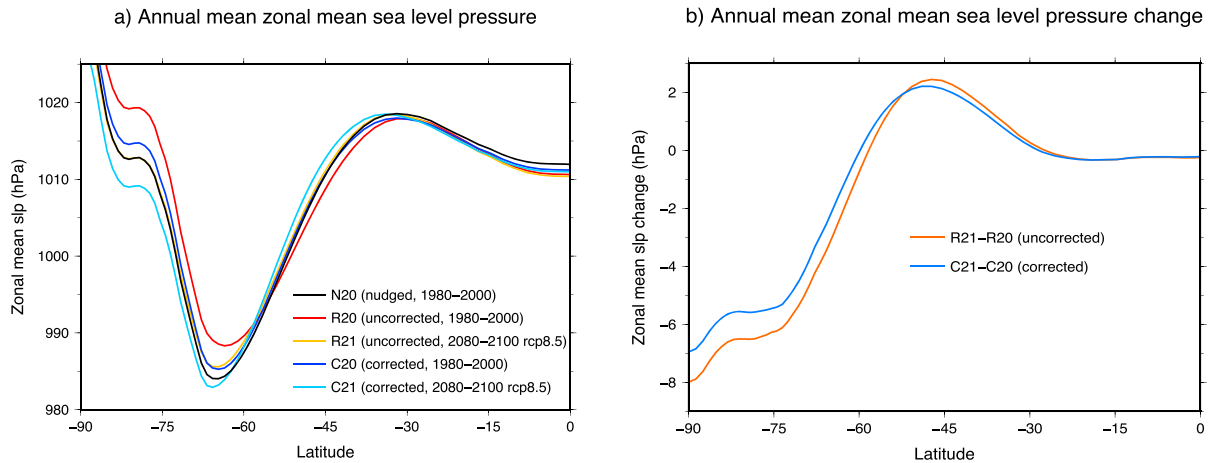


Figure 12. Annual mean zonal mean sea-level pressure (hPa) for the different LMDZ simulations (late 20th and late 21st centuries). (a) Absolute values and (b) difference between the late 20th and late 21st centuries in the two sets of simulations (corrected and uncorrected).

and C21: In the bias-corrected simulation, the trough is located about 2° latitude further south and about 3 hPa deeper. By coincidence, the location and intensity of the pressure trough in the corrected end 20th century simulation C20 are almost identical to its location and intensity in the uncorrected end 21st century simulation R21. Climate change leads to the same displacement and intensification of the pressure trough in the corrected and uncorrected simulation sets. In other words, a similar geographic shift occurs in both sets of simulations in terms of amplitude and displacement, but not in terms of localization of the shift (see Figure 12b, which shows that the maximum pressure increase occurs further south in the corrected set of simulations). This means that the bias correction, which is the same for both periods, does not “pin” circulation features. Such a “pinning” effect might occur if a given circulation feature (e.g., a low-level jet) is badly represented in an uncorrected model, and the correction terms are of the order of magnitude of the feature itself. In that case, moderate shifts in location and magnitude of that feature, induced by changing climatic conditions, could be overridden by the large static bias correction terms. However, when the model error (and thus the bias correction) is only of similar magnitude as the projected change (which is often the case and also the case here), this does not occur.

In spite of the differences in the location of the low-pressure trough, the spatial pattern of sea level pressure change between the two periods is very similar in the corrected (C21–C20) and uncorrected set (R21–R20) of simulations (Figure 13). This is expected as the simulated climate change, in particular over the Southern

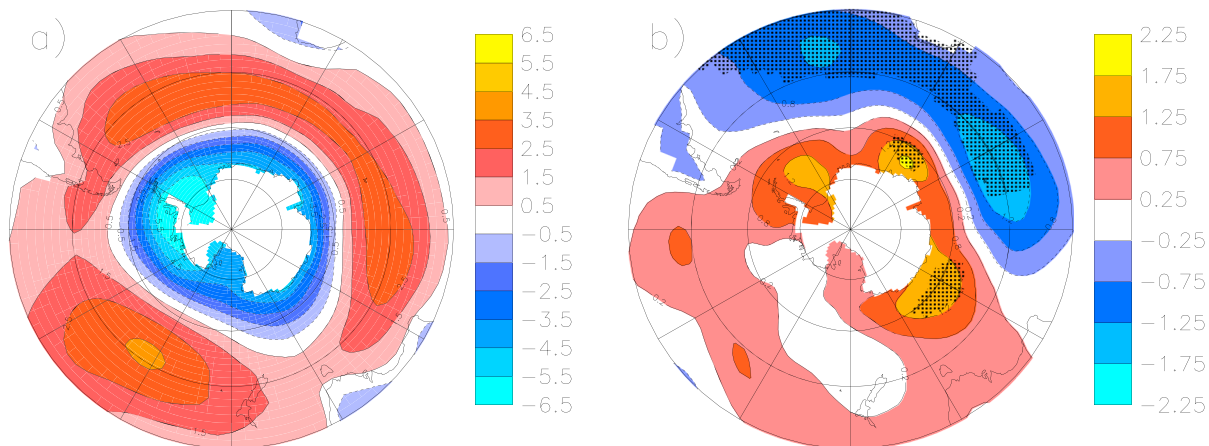


Figure 13. Projected change (1980–2000 vs. 2080–2100) of annual mean sea-level pressure and its sensitivity to bias correction. (a) Projected change of annual mean sea-level pressure in the uncorrected set of simulations (R21–R20), in hPa. (b) Sensitivity of this projected change to bias correction ([C21–C20]–[R21–R20]), in hPa. Note the change of scale between (a) and (b). In (b), stippling indicates statistically significant changes at the 95% level.

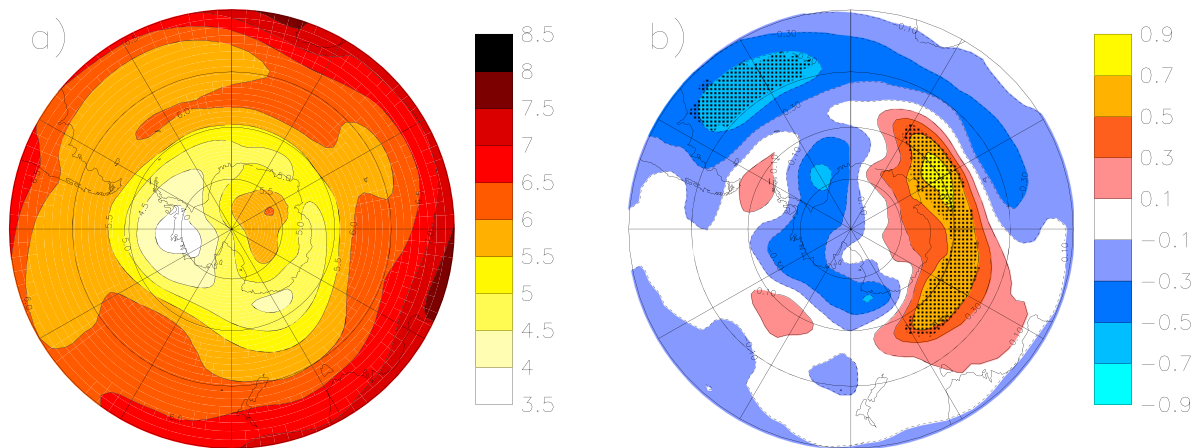


Figure 14. Projected change (1980–2000 vs. 2080–2100) of annual 500-hPa temperature and its sensitivity to bias correction. (a) Projected change of annual mean 500-hPa temperature in the uncorrected set of simulations (R21–R20), in °C. (b) Sensitivity of this projected change to bias correction ($[C21-C20]-[R21-R20]$, in °C). In (b), stippling indicates statistically significant changes at the 95% level.

Ocean, is essentially constrained by the prescribed SST and SIC change (Krinner et al., 2014), which is the same in both sets of simulations. Nevertheless, the intensification of the large-scale meridional pressure gradient between the temperate and polar regions is significantly attenuated in the bias-corrected simulations (Figure 13b).

The projected midtropospheric temperature change (Figure 14) exhibits an essentially zonal signal in both sets of simulations, with a much weaker 500 hPa warming over Antarctica than at lower latitudes (Figure 14a), as projected already in early transient climate change simulations with sufficiently detailed fully coupled models (Stouffer et al., 1989). Slight but significant (95% in a double-sided t test) differences, amounting locally to about 20% of the projected warming, can be seen between the two sets of simulations (Figure 14b); these seem to be linked to the differential circulation changes shown in Figure 13b. Over the continent, the midtropospheric temperature is only very weakly affected by the bias correction. Similarly, the simulated surface air temperature change over the Antarctic ice sheet is not substantially affected by the bias corrections (about +4.7 °C in both the corrected and uncorrected sets of simulations).

The large-scale geographic pattern of projected precipitation change is again similar in the corrected and uncorrected sets of simulations (Figure 15). There is no precipitation increase over the Ross Ice Shelf area. This is probably linked to the simulated sea level pressure change (Figure 13), which indicates stronger cold

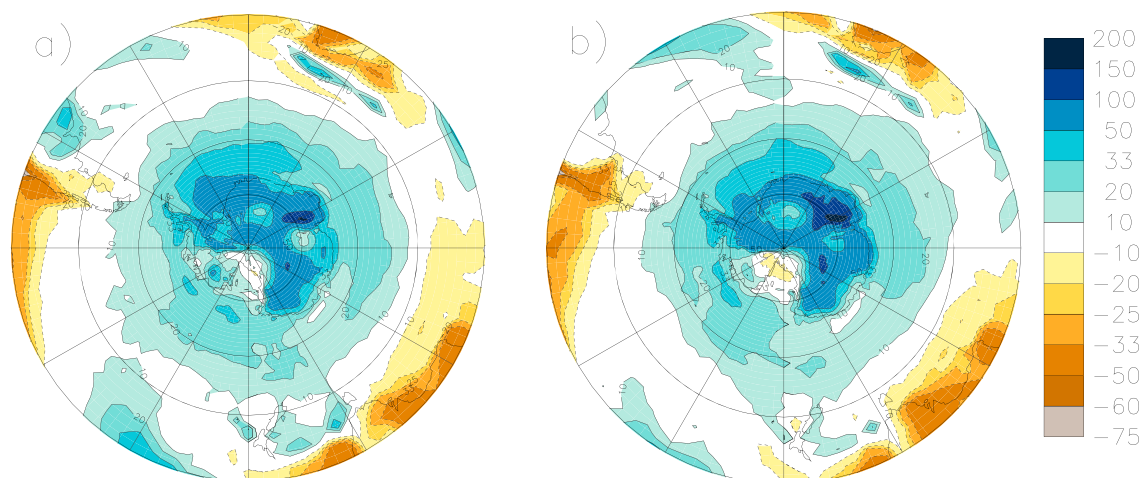


Figure 15. Projected relative change (1980–2000 vs. 2080–2100) of annual precipitation (in %). (a) Uncorrected set of simulations: $([R21-R20]/R20)$; (b) corrected set of simulations: $([C21-C20]/C20)$.

air advection to that sector from the interior of West Antarctica at the end of the 21st century. Precipitation increase is substantial over the rest of the continent, both in the corrected and uncorrected version of LMDZ.

The relative continental mean precipitation change is largely unaffected by the bias correction. It is +38% in the uncorrected runs (in absolute terms, an increase of continental average precipitation from 193 in R20 to 266 kg·m⁻²·year in R21, including present ice shelves) and +41% in the corrected ones (an increase from 179 to 253 kg·m⁻²·year, again including present ice shelves). As the projected surface air temperature increase is also weakly sensitive to the bias correction, the continental-scale accumulation (precipitation minus sublimation) sensitivity to warming in both versions is similar (6.4%/°C in the uncorrected version and 6.9%/°C in the corrected version). Although both seem somewhat high compared to independent estimates of about (5 ± 1)%/°C (Frieler et al., 2015), they agree well with previous versions of LMDZ (Krinner et al., 2008) and, more importantly, other global climate models (Frieler et al., 2015; Meehl et al., 2007).

In terms of surface mass balance, the projected future precipitation increase is partially compensated for by increased melt rates, and by an increased fraction of liquid precipitation in both model versions (corrected and uncorrected). As mentioned before, the corrected version (C20 and C21) is somewhat colder than the uncorrected one (R20 and R21). However, this does not substantially affect the fraction of meltwater that refreezes, as diagnosed following Pfeffer et al. (1991) and Thompson and Pollard (1997). This diagnosed fraction is about 50% in R20 and C20 and decreases to about 30% in the warmer future climate both in R21 and C21. As a whole, the effects of the bias correction on the projected changes of the different surface mass balance terms (snowfall, rainfall and its partial runoff, meltwater generation and refreezing, sublimation) almost perfectly compensate for each other. As a consequence, the continental-mean simulated average surface mass balance increase (including ice shelf areas) is 69 kg·m⁻²·year in the simulations with atmospheric bias correction (C21-C20), and almost identical (68 kg·m⁻²·year) in the simulations without (R21-R20). A more detailed analysis would require simulations at higher spatial resolution in order to better resolve in particular the steep ice sheet margins.

4. Discussion

4.1. Why Bias Corrections?

In climate change impact studies, bias correction is usually carried out at some stage (Maraun, 2016); in most cases, bias correction is carried out on climate model output (e.g., Ehret et al., 2012). This is also frequently the case in asymmetric coupling exercises, such as coupling of ice sheet models to atmospheric models (e.g., Herrington & Poulsen, 2012; Quiquet et al., 2012). As long as coupled climate models do simulate a substantially biased present-day climate—the amplitude of the biases is typically of the order of the expected climate change on a centennial timescale (Flato et al., 2013)—bias correction appears inevitable at some stage, if useful assessments of future climatic conditions and their impacts on natural and human systems are to be produced. At the current state of the art, the essential question is not that much whether bias correction is required at some stage, but rather at which stage, and how it is to be implemented.

Concerning specifically the type of bias correction approach used here (often also termed “flux corrections”), Dommenget and Reznay (2018) recently showed that in some respects, it can be preferable over model tuning, because it can be “much cheaper, simpler, more transparent and it does not introduce artificial error interactions between submodels.”

4.2. Bias Stationarity: A Necessary and Sufficient Condition for Corrected Projections

All bias correction methods implicitly assume, or explicitly postulate, that climate model biases are either constant in time, or consistently dependent on the climate state (Buser et al., 2009; Déqué, 2007; Kerkhoff et al., 2014). These assumptions have primarily been evaluated for near-surface air temperatures and precipitation rates, and at temporal and spatial scales relevant for climate change impact studies.

The bias correction method used here for simulations of the present and possible future climate applies to comparatively large spatial (AGCM scale) and temporal (monthly) scales, and it applies to atmospheric circulation parameters (temperature and winds above the atmospheric boundary layer) rather than to near-surface parameters directly relevant for impact studies. Stability in time of large-scale bias patterns is the primary condition for the validity of this type of bias correction. Strong stationarity of atmospheric biases

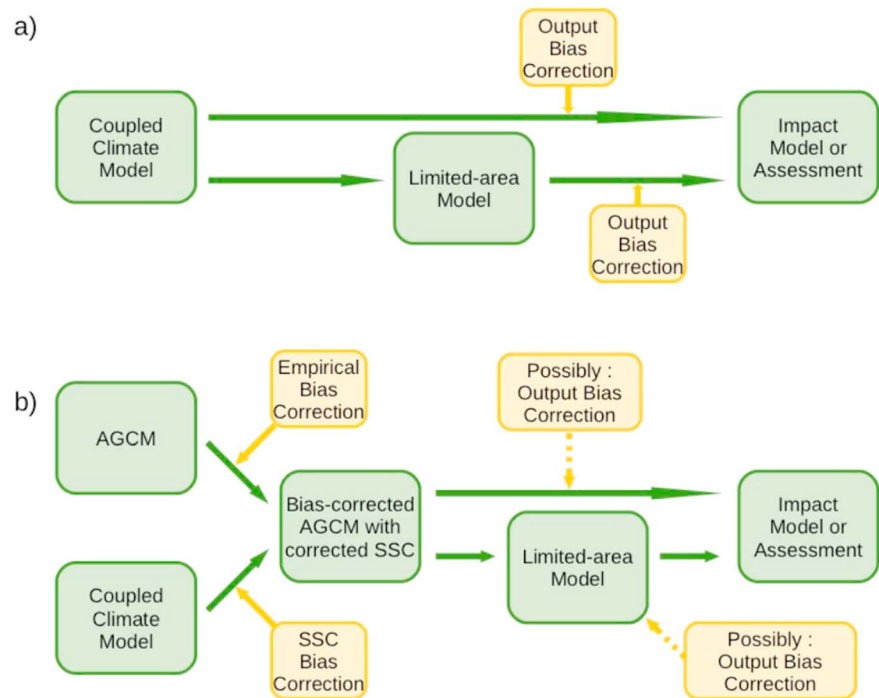


Figure 16. Climate impact modeling chain. (a) Classical flow and (b) alternative flow including bias-corrected AGCM simulations, optionally including limited-area model simulations and bias correction immediately before the impact modeling step.

has recently been shown by Krinner and Flanner (2018). This provides the required confidence in the applicability of this type of empirical bias correction to AGCM simulations of climate change.

Climate change as simulated by an atmospheric model is very tightly constrained by the prescribed SST and SIC change (Krinner et al., 2014). Therefore, the flux correction that we advocate for should be applied in conjunction with a complementary correction of OBC, such as a quantile-quantile method for sea ice and SST that was assessed by Beaumet et al. (2017). It would not make much sense to correct atmospheric circulation patterns without insuring that the forcing of the AGCM at its lower oceanic boundaries is debiased in a consistent manner.

4.3. Use of Bias-Corrected AGCM Simulations as Boundary Conditions for RCMs and as Input for Climate Change Impact Studies

The method for bias-corrected regional-scale climate projections with an AGCM presented here represents a substantial step further compared to a previous study (Krinner et al., 2014) in which only bias-corrected OBC were used. In the present study, we have bias-corrected the atmospheric temperature and winds, and in addition, we have applied an improved OBC correction method (Beaumet et al., 2017).

The climate impact assessment chain typically consists of a coupled climate model, a limited-area climate model or a statistic downscaling procedure, and impact models or models of other natural systems (e.g., an ice sheet model for sea level change projections) further downstream (Figure 16a). Here we propose to insert an intermediate step after the coupled climate model: a bias-corrected atmospheric GCM that can either replace a limited-area model if run at sufficiently high (regional or global) resolution or serve as driver for a limited-area climate model or a statistical downscaling procedure (Figure 16b).

The various bias correction methods of climate model output are often criticized for the physical inconsistency and the nonpreservation of the multivariate correlation structure between the different variables that they are applied to (Sippel et al., 2016). In addition, it is clear that an a posteriori bias correction (often termed bias adjustment) of climate model output cannot correct for atmospheric circulation biases (potentially leading to an implicit pinning of atmospheric circulation features), yielding unphysical corrections

that raise doubt about the credibility of the adjusted output (Maraun et al., 2017). Perfect physical consistency between all atmospheric variables is not guaranteed either with the empirical bias correction method used here, as empirical correction terms are added to the prognostic equations for some key variables (here temperature and wind). However, the state of the simulated atmosphere immediately adjusts to these small continuous corrections, preserving a high degree of physical consistency across the representation of the atmospheric processes. We have shown in this paper that atmospheric circulation biases, which can severely compromise usual a posteriori bias corrections particularly when circulation patterns are misplaced (Maraun et al., 2017), can be efficiently corrected using empirical runtime bias correction. This approach therefore allows producing a consistent depiction of regional climate change with a wide range of potential uses and applications, either as boundary conditions for a limited-area, high-resolution climate model or directly as an input for climate change impact models.

An additional bias correction of regional climate model output for impact models downstream might nevertheless remain necessary (Figure 16b). There is, in fact, an obvious complementarity, and potentially a substantial synergy, between the empirical run-time bias corrections of climate models, which we carried out here, and a secondary climate model output bias adjustment (in conjunction with downscaling to spatial scales relevant for impact models) at a later stage. Because the usual statistical bias adjustment of climate model output cannot correct for climate model circulation biases and can be severely and adversely impacted by these (Maraun et al., 2017), the empirical run-time climate model bias correction carried out here can even be seen as a potential condition for meaningful statistical climate model output adjustment before the impact modeling step. In addition, one might deem preferable to apply several small bias corrections at different phases of the modeling chain instead of one large correction at the end.

Given the substantial computational cost of high-resolution limited area model simulations, driving these models with biased atmospheric boundary conditions, which necessarily lead to biased output (the garbage in-garbage out problem), is problematic. The procedure suggested here circumvents this drawback, or at least considerably alleviates it.

4.4. Stretched-Grid Variable Resolution Versus Regular Grid Simulations

For the sake of computational efficiency in this “proof-of-concept” study, we have chosen to run the bias-corrected AGCM in a stretched grid configuration with about 100-km horizontal resolution over the region of interest and very moderate to low resolution in the Northern Hemisphere. Running the bias-corrected AGCM at a global high resolution of about 50 km (a resolution typically used in the HighResMIP exercise; Haarsma et al., 2016), and using the output of these simulations to drive a regional climate model at an even higher resolution, appears to be an attractive solution, because these simulations can be used to drive RCMs over any region of the globe. Alternatively, the bias-corrected AGCM can be used in stretched-grid configuration if the AGCM has that capacity and the simulated near-surface climate compares well with observations. In this case, the drawback that the output can be used only for climate change studies over the chosen high-resolution region is compensated for by the reduced computational cost of the AGCM runs. Specifically for the Antarctic, Genthon et al. (2009) have shown that simulated precipitation and precipitation change are highly sensitive to model resolution, justifying the stretched-grid approach at least in the context of studies of the Antarctic climate change because of the global impacts of changes of the Antarctic surface mass balance.

5. Conclusions

The empirical run-time bias correction method used here, sometimes referred to as “flux correction,” is a cost-effective means of producing almost bias-free, physically consistent AGCM simulations of the present-day climate (Guldberg et al., 2005; Kharin & Scinocca, 2012). In this work, we have shown a strong positive effect of applying this bias correction method on the simulation of the present Antarctic climate on daily to interannual timescales.

Strong and systematic stationarity of large-scale coupled climate model biases during climate change, recently shown by Krinner and Flanner (2018), opens up the possibility to use empirical AGCM bias correction for AGCM climate change simulations. The AGCM climate change simulations carried out here used bias-corrected OBC (Beaumont et al., 2017; Krinner et al., 2008) and an empirical bias correction of

atmospheric temperatures and winds. The simulated change of atmospheric circulation features is physically self-consistent and in many respects very similar to the climate change simulated in uncorrected simulations. At the same time, geographical shifts of circulation features under climate change are consistently represented in the bias-corrected simulations, and there is no indication that the empirical bias-correction method pins these features to a given position.

As a whole, this empirical bias-correction method is a key element of an attractive alternative, or complement, to the “classical” climate change impact modeling chain. There is indeed a strong complementarity and large potential for synergy between the generic “upstream” empirical run-time bias correction applied here and the usual, often application-specific, “downstream” climate model output bias adjustment. This method should be more thoroughly tested in the future, in particular with (stretched or regular-grid) high-resolution AGCM configurations and/or in a pseudo-reality framework.

Acknowledgments

The Agence Nationale de la Recherche funded this study through contracts ANR-14-CE01-0001 (ASUMA), ANR-15-CE01-0003 (APRES3), and ANR-15-CE01-0015 (AC-AHC2). This work was performed using HPC resources from GENCI-IDRIS (Grant 2017-A0020100239). Output from our simulations can be obtained on the IDRIS DODS server as described in https://prodn.idris.fr/thredds/fileServer/ipsl_public/rcses604/KrinnerEA_JAMES_2018MS001438/README. Gwenn Le Normand contributed to analyses of preliminary results. We thank John Scinocca, Slava Kharin, Hubert Gallée, Christophe Genthon, Bill Gutowski, Bill Merryfield, and François Engelbrecht for insightful discussions and suggestions.

References

- Agosta, C., Favier, V., Krinner, G., Gallée, H., Fettweis, X., & Genthon, C. (2013). High-resolution modelling of the Antarctic surface mass balance, application for the twentieth, twenty first and twenty second centuries. *Climate Dynamics*, *41*(11–12), 3247–3260. <https://doi.org/10.1007/s00382-013-1903-9>
- Agosta, C., Fettweis, X., & Datta, R. (2015). Evaluation of the CMIP5 models in the aim of regional modelling of the Antarctic surface mass balance. *The Cryosphere*, *9*(6), 2311–2321. <https://doi.org/10.5194/tc-9-2311-2015>
- Ashfaq, M., Skinner, C. B., & Diffenbaugh, N. S. (2011). Influence of SST biases on future climate change projections. *Climate Dynamics*, *36*(7–8), 1303–1319. <https://doi.org/10.1007/s00382-010-0875-2>
- Beaumont, J., Krinner, G., Déqué, M., Haarsma, R., & Li, L. (2017). Assessing bias-corrections of oceanic surface conditions for atmospheric models. *Geoscientific Model Development Discussion*, 1–29. <https://doi.org/10.5194/gmd-2017-247>
- Bruyère, C. L., Done, J. M., Holland, G. J., & Fredrick, S. (2013). Bias corrections of global models for regional climate simulations of high-impact weather. *Climate Dynamics*, *43*(7–8), 1847–1856. <https://doi.org/10.1007/s00382-013-2011-6>
- Buser, C. M., Künsch, H. R., Lüthi, D., Wild, M., & Schär, C. (2009). Bayesian multi-model projection of climate: Bias assumptions and interannual variability. *Climate Dynamics*, *33*(6), 849–868. <https://doi.org/10.1007/s00382-009-0588-6>
- Chen, J., Brissette, F. P., & Lucas-Picher, P. (2015). Assessing the limits of bias-correcting climate model outputs for climate change impact studies. *Journal of Geophysical Research: Atmospheres*, *120*, 112–1136. <https://doi.org/10.1002/2014JD022635>
- Collins, M., Booth, B. B. B., Harris, G. R., Murphy, J. M., Sexton, D. M. H., & Webb, M. J. (2006). Towards quantifying uncertainty in transient climate change. *Climate Dynamics*, *27*(2–3), 127–147. <https://doi.org/10.1007/s00382-006-0121-0>
- Collins, M., Knutti, R., Arblaster, J., Dufresne, J.-L., Fichefet, T., Friedlingstein, P., et al. (2013). Long-term climate change: Projections, commitments and irreversibility. In *Climate change 2013: The physical science basis. Contribution of Working Group I to the Fifth Assessment Report of the Intergovernmental Panel on Climate Change* (pp. 1029–1136). New York, NY: Cambridge University Press. <https://doi.org/10.1017/CBO9781107415324.024>
- Cornford, S. L., Martin, D. F., Payne, A. J., Ng, E. G., Le Brocq, A. M., Gladstone, R. M., et al. (2015). Century-scale simulations of the response of the West Antarctic Ice Sheet to a warming climate. *The Cryosphere*, *9*(4), 1579–1600. <https://doi.org/10.5194/tc-9-1579-2015>
- Dee, D. P., Uppala, S. M., Simmons, A. J., Berrisford, P., Poli, P., Kobayashi, S., et al. (2011). The ERA-interim reanalysis: Configuration and performance of the data assimilation system. *Quarterly Journal of the Royal Meteorological Society*, *137*(656), 553–597. <https://doi.org/10.1002/qj.828>
- Déqué, M. (2007). Frequency of precipitation and temperature extremes over France in an anthropogenic scenario: Model results and statistical correction according to observed values. *Global and Planetary Change*, *57*(1–2), 16–26. <https://doi.org/10.1016/j.gloplacha.2006.11.030>
- Dommenget, D., & Rezný, M. (2018). A caveat note on tuning in the development of coupled climate models. *Journal of Advances in Modeling Earth Systems*, *10*, 78–97. <https://doi.org/10.1002/2017MS000947>
- Done, J. M., Holland, G. J., Bruyère, C. L., Leung, L. R., & Suzuki-Parker, A. (2015). Modeling high-impact weather and climate: Lessons from a tropical cyclone perspective. *Climatic Change*, *129*(3–4), 381–395. <https://doi.org/10.1007/s10584-013-0954-6>
- Driouech, F., Déqué, M., & Sánchez-Gómez, E. (2010). Weather regimes-Moroccan precipitation link in a regional climate change simulation. *Global and Planetary Change*, *72*(1–2), 1–10. <https://doi.org/10.1016/j.gloplacha.2010.03.004>
- Dufresne, J. L., Foujols, M. A., Denvil, S., Caubel, A., Marti, O., Aumont, O., et al. (2013). Climate change projections using the IPSL-CM5 earth system model: From CMIP3 to CMIP5. *Climate Dynamics*, *40*(9–10), 2123–2165. <https://doi.org/10.1007/s00382-012-1636-1>
- Ehret, U., Zehe, E., Wulfmeyer, V., Warrach-Sagi, K., & Liebert, J. (2012). HESS opinions “should we apply bias correction to global and regional climate model data?”. *Hydrology and Earth System Sciences*, *16*(9), 3391–3404. <https://doi.org/10.5194/hess-16-3391-2012>
- Favier, V., Krinner, G., Amory, C., Gallée, H., Beaumont, J., & Agosta, C. (2017). Antarctica-regional climate and surface mass budget. *Current Climate Change Reports*, *3*, 303–315. <https://doi.org/10.1007/s40641-017-0072-z>
- Flato, G., Marotzke, J., Abiodun, B., Braconnot, P., Chou, S. C., Collins, W., et al. (2013). Evaluation of climate models. In *Climate change 2013: The physical science basis. Contribution of Working Group I to the Fifth Assessment Report of the Intergovernmental Panel on Climate Change* (pp. 741–866). Cambridge, UK: Cambridge University Press. <https://doi.org/10.1017/CBO9781107415324>
- Frieler, K., Clark, P. U., He, F., Buizert, C., Reese, R., Ligtenberg, S. R. M., et al. (2015). Consistent evidence of increasing Antarctic accumulation with warming. *Nature Climate Change*, *5*(4), 348–352. <https://doi.org/10.1038/nclimate2574>
- Genthon, C., Krinner, G., & Castebrunet, H. (2009). Antarctic precipitation and climate-change predictions: Horizontal resolution and margin vs plateau issues. *Annals of Glaciology*, *50*(50), 55–60. <https://doi.org/10.3189/172756409787769681>
- Giorgi, F., & Gutowski, W. J. (2015). Regional dynamical downscaling and the CORDEX initiative. *Annual Review of Environment and Resources*, *40*(1), 467–490. <https://doi.org/10.1146/annurev-environ-102014-021217>
- Gleckler, P. J., Taylor, K. E., & Doutriaux, C. (2008). Performance metrics for climate models. *Journal of Geophysical Research*, *113*, D06104. <https://doi.org/10.1029/2007JD008972>

- Gulberg, A., Kaas, E., Déqué, M., Yang, S., & Vester Thorsen, S. (2005). Reduction of systematic errors by empirical model correction: Impact on seasonal prediction skill. *Tellus Series A: Dynamic Meteorology and Oceanography*, *57*(4), 575–588. <https://doi.org/10.1111/j.1600-0870.2005.00120.x>
- Gutowski, J. W., Giorgi, F., Timbal, B., Frigon, A., Jacob, D., Kang, H. S., et al. (2016). WCRP COordinated Regional Downscaling EXperiment (CORDEX): A diagnostic MIP for CMIP6. *Geoscientific Model Development*, *9*(11), 4087–4095. <https://doi.org/10.5194/gmd-9-4087-2016>
- Haarsma, R. J., Roberts, M. J., Vidale, P. L., Catherine, A., Bellucci, A., Bao, Q., et al. (2016). High resolution model intercomparison project (HighResMIP v1.0) for CMIP6. *Geoscientific Model Development*, *9*(11), 4185–4208. <https://doi.org/10.5194/gmd-9-4185-2016>
- Haerter, J. O., Hagemann, S., Moseley, C., & Piani, C. (2011). Climate model bias correction and the role of timescales. *Hydrology and Earth System Sciences*, *15*(3), 1065–1079. <https://doi.org/10.5194/hess-15-1065-2011>
- Hall, A. (2014). Projecting regional change. *Science*, *346*(6216), 1461–1462. <https://doi.org/10.1126/science.aaa0629>
- Hernández-Díaz, L., Laprise, R., Nikiéma, O., & Winger, K. (2017). 3-step dynamical downscaling with empirical correction of sea-surface conditions: Application to a CORDEX Africa simulation. *Climate Dynamics*, *48*(7–8), 2215–2233. <https://doi.org/10.1007/s00382-016-3201-9>
- Herrington, A. R., & Poulsen, C. J. (2012). Terminating the last interglacial: The role of ice sheet-climate feedbacks in a GCM asynchronously coupled to an ice sheet model. *Journal of Climate*, *25*(6), 1871–1882. <https://doi.org/10.1175/JCLI-D-11-00218.1>
- Hewitson, B. C., Daron, J., Crane, R. G., Zermoglio, M. F., & Jack, C. (2014). Interrogating empirical-statistical downscaling. *Climatic Change*, *122*(4), 539–554. <https://doi.org/10.1007/s10584-013-1021-z>
- Hourdin, F., Foujols, M. A., Codron, F., Guemas, V., Dufresne, J. L., Bony, S., et al. (2013). Impact of the LMDZ atmospheric grid configuration on the climate and sensitivity of the IPSL-CM5A coupled model. *Climate Dynamics*, *40*(9–10), 2167–2192. <https://doi.org/10.1007/s00382-012-1411-3>
- Irvine, P. J., Gregoire, L. J., Lunt, D. J., & Valdes, P. J. (2013). An efficient method to generate a perturbed parameter ensemble of a fully coupled AOGCM without flux-adjustment. *Geoscientific Model Development*, *6*(5), 1447–1462. <https://doi.org/10.5194/gmd-6-1447-2013>
- Jeuken, A. B. M., Siegmund, P. C., Heijboer, L. C., Feichter, J., & Bengtsson, L. (1996). On the potential of assimilating meteorological analyses in a global climate model for the purpose of model validation. *Journal of Geophysical Research*, *101*(D12), 16,939–16,950. <https://doi.org/10.1029/96JD01218>
- Kerkhoff, C., Künsch, H. R., & Schär, C. (2014). Assessment of bias assumptions for climate models. *Journal of Climate*, *27*(17), 6799–6818. <https://doi.org/10.1175/JCLI-D-13-00716.1>
- Kharin, V. V., & Scinocca, J. F. (2012). The impact of model fidelity on seasonal predictive skill. *Geophysical Research Letters*, *39*, L18803. <https://doi.org/10.1029/2012GL052815>
- Kohonen, T. (1990). The self-organizing map. *Proceedings of the IEEE*, *78*(9), 1464–1480. <https://doi.org/10.1109/5.58325>
- Kohonen, T., & Honkela, T. (2007). Kohonen network. *Scholarpedia*, *2*(1), 1568. <https://doi.org/10.4249/scholarpedia.1568>
- Krinner, G., & Flanner, M. G. (2018). Striking stationarity of large-scale climate model bias patterns under strong climate change. *Proceedings of the National Academy of Sciences*, *115*(38), 9462–9466. <https://doi.org/10.1073/pnas.1807912115>
- Krinner, G., Guicherd, B., Ox, K., Genthon, C., & Magand, O. (2008). Influence of oceanic boundary conditions in simulations of antarctic climate and surface mass balance change during the coming century. *Journal of Climate*, *21*(5), 938–962. <https://doi.org/10.1175/2007JCLI1690.1>
- Krinner, G., Llargeron, C., Ménégou, M., Agosta, C., & Brutel-Vuilmet, C. (2014). Oceanic forcing of Antarctic climate change: A study using a stretched-grid atmospheric general circulation model. *Journal of Climate*, *27*(15), 5786–5800. <https://doi.org/10.1175/JCLI-D-13-00367.1>
- Ma, H. Y., Xie, S., Klein, S. A., Williams, K. D., Boyle, J. S., Bony, S., et al. (2014). On the correspondence between mean forecast errors and climate errors in CMIP5 models. *Journal of Climate*, *27*(4), 1781–1798. <https://doi.org/10.1175/JCLI-D-13-00474.1>
- Manabe, S., & Stouffer, R. (1988). Two stable equilibria of a coupled ocean-atmosphere model. *Journal of Climate*, *1*(9), 841–866. [https://doi.org/10.1175/1520-0442\(1988\)001<0841:TSEOAC>2.0.CO;2](https://doi.org/10.1175/1520-0442(1988)001<0841:TSEOAC>2.0.CO;2)
- Maraun, D. (2016). Bias correcting climate change simulations—A critical review. *Current Climate Change Reports*, *2*(4), 211–220. <https://doi.org/10.1007/s40641-016-0050-x>
- Maraun, D., Shepherd, T. G., Widmann, M., Zappa, G., Walton, D., Gutiérrez, J. M., et al. (2017). Towards process-informed bias correction of climate change simulations. *Nature Climate Change*, *7*(11), 664–773. <https://doi.org/10.1038/nclimate3418>
- Meehl, G. A., Stocker, T. F., Collins, W. D., Friedlingstein, P., Gaye, A. T., Gregory, J. M., et al. (2007). Global climate projections. In S. Solomon et al. (Eds.), *In climate change 2007: The physical science basis. Contribution of Working Group I to the Fourth Assessment Report of the Intergovernmental Panel on Climate Change* (pp. 748–844). Cambridge: Cambridge University Press.
- Mo, K. C., & Higgins, R. W. (1998). The Pacific–South American modes and tropical convection during the Southern Hemisphere winter. *Monthly Weather Review*, *126*(6), 1581–1596. [https://doi.org/10.1175/1520-0493\(1998\)126<1581:TPSAMA>2.0.CO;2](https://doi.org/10.1175/1520-0493(1998)126<1581:TPSAMA>2.0.CO;2)
- Patricola, C. M., & Cook, K. H. (2010). Northern African climate at the end of the twenty-first century: An integrated application of regional and global climate models. *Climate Dynamics*, *35*(1), 193–212. <https://doi.org/10.1007/s00382-009-0623-7>
- Pfeffer, W. T., Meier, M. F., & Illangasekare, T. H. (1991). Retention of Greenland runoff by refreezing: Implications for projected future sea level change. *Journal of Geophysical Research*, *96*(C12), 22,117–22,124. <https://doi.org/10.1029/91JC02502>
- Quiquet, A., Punge, H. J., Ritz, C., Fettweis, X., Gallée, H., Kageyama, M., et al. (2012). Sensitivity of a Greenland ice sheet model to atmospheric forcing fields. *The Cryosphere*, *6*(5), 999–1018. <https://doi.org/10.5194/tc-6-999-2012>
- Rayner, N. A., Parker, D. E., Horton, E. B., Folland, C. K., Alexander, L. V., Rowell, D. P., et al. (2003). Global analyses of sea surface temperature, sea ice, and night marine air temperature since the late nineteenth century. *Journal of Geophysical Research*, *108*(D14), 4407. <https://doi.org/10.1029/2002JD002670>
- Rummukainen, M. (2010). State-of-the-art with regional climate models. *Wiley Interdisciplinary Reviews: Climate Change*, *1*(1), 82–96. <https://doi.org/10.1002/wcc.8>
- Sausen, R., Barthel, K., & Hasselmann, K. (1988). Coupled ocean-atmosphere models with flux correction. *Climate Dynamics*, *2*(3), 145–163. <https://doi.org/10.1007/BF01053472>
- Shepherd, A., Ivins, E., Rignot, E., Smith, B., Van Den Broeke, M., Velicogna, I., et al. (2018). Mass balance of the Antarctic Ice Sheet from 1992 to 2017. *Nature*, *558*(7709), 219–222. <https://doi.org/10.1038/s41586-018-0179-y>
- Sippel, S., Otto, F. E. L., Forkel, M., Allen, M. R., Guillod, B. P., Heimann, M., et al. (2016). A novel bias correction methodology for climate impact simulations. *Earth System Dynamics*, *7*(1), 71–88. <https://doi.org/10.5194/esd-7-71-2016>
- Stouffer, R. J., Manabe, S., & Bryan, K. (1989). Interhemispheric asymmetry in climate response to a gradual increase of atmospheric CO₂. *Nature*, *338*, 660–662. <https://doi.org/10.1016/B978-0-444-88351-3.50016-7>

- Teutschbein, C., & Seibert, J. (2013). Is bias correction of regional climate model (RCM) simulations possible for non-stationary conditions. *Hydrology and Earth System Sciences*, *17*(12), 5061–5077. <https://doi.org/10.5194/hess-17-5061-2013>
- Thompson, S. L., & Pollard, D. (1997). Greenland and Antarctic mass balances for present and doubled atmospheric CO₂ from the GENESIS version-2 global climate model. *Journal of Climate*, *10*(5), 871–900. [https://doi.org/10.1175/1520-0442\(1997\)010<0871:GAAMBF>2.0.CO;2](https://doi.org/10.1175/1520-0442(1997)010<0871:GAAMBF>2.0.CO;2)
- Xu, Z., & Yang, Z. L. (2012). An improved dynamical downscaling method with GCM bias corrections and its validation with 30 years of climate simulations. *Journal of Climate*, *25*(18), 6271–6286. <https://doi.org/10.1175/JCLI-D-12-00005.1>
- Yukimoto, S., Adachi, Y., Hosaka, M., Sakami, T., Yoshimura, H., Hirabara, M., et al. (2012). A new global climate model of the meteorological research institute: MRI-CGCM3 -model description and basic performance. *Journal of the Meteorological Society of Japan*, *90A*, 23–64. <https://doi.org/10.2151/jmsj.2012-A02>